PHOTONICS Research

MXene-$Ti_3C_2T_x$ for watt-level high-efficiency pulse generation in a 2.8 μm mid-infrared fiber laser

CHEN WEI,[1,*] LIQIANG ZHOU,[2] DONGSHENG WANG,[1,3] HAO CHI,[1] HUA HUANG,[2] HAN ZHANG,[2,4] AND YONG LIU[1]

[1]State Key Laboratory of Electronic Thin Films and Integrated Devices, School of Optoelectronic Science and Engineering, University of Electronic Science and Technology of China, Chengdu 610054, China
[2]College of Electrical Engineering, Sichuan University, Chengdu 610065, China
[3]e-mail: wangds@uestc.edu.cn
[4]e-mail: hanz@scu.edu.cn
*Corresponding author: cwei@uestc.edu.cn

Received 23 January 2020; revised 27 March 2020; accepted 8 April 2020; posted 9 April 2020 (Doc. ID 388930); published 29 May 2020

We report a watt-level passively *Q*-switched 2.8 μm mid-infrared multi-mode fiber laser by employing multi-layered two-dimensional MXene-$Ti_3C_2T_x$ as the saturable absorber (SA). The MXene-$Ti_3C_2T_x$ is fabricated by selectively etching aluminum layers in Ti_3AlC_2. The non-saturable loss, modulation depth, and saturable intensity of the SA at 2866 nm were measured to be 25.0%, 33.2%, and 0.043 GW/cm^2, respectively. The maximum average output power of the $Ti_3C_2T_x$ *Q*-switched fiber laser reached 1.09 W at 28.23% slope efficiency. The pulse repetition rate, shortest pulse width, pulse peak power, and single-pulse energy were 78.12 kHz, 1.04 μs, 13.4 W, and 13.93 μJ, respectively. This is the first demonstration of watt-level pulse generation in a mid-infrared fiber laser using low dimensional materials, to the best of our knowledge. These results indicate that the $Ti_3C_2T_x$ is a reliable and superior broadband SA for high power mid-infrared pulsed laser generation.

https://doi.org/10.1364/PRJ.388930

1. INTRODUCTION

High power pulsed fiber laser sources operating in the 3 μm mid-infrared spectral region have drawn significant attention in the past decade attributed to their growing number of advanced applications in spectroscopy [1], infrared countermeasures [2], and biological tissue ablation [3], as well as their numerous advantages, including compact design, outstanding beam quality, high conversion efficiency, flexibility, efficient heat dissipation, and great potential for power scaling [4], over other types of mid-infrared sources. Mid-infrared *Q*-switched fiber laser sources capable of delivering laser pulses with high average power and pulse energy have been realized by active, passive, and hybrid approaches [5–7]. Compared with other technologies, the passive method employing saturable absorbers (SAs) possesses merits of simplicity, low-cost, and compactness.

While many kinds of materials have been considered as SAs for mid-infrared pulsed fiber laser, there is a particular demand for two-dimensional (2D) layered materials-based mid-infrared pulse generation. This is due to that they overcome the inherent drawbacks, namely a complicated manufacture process, high cost, and narrow operational waveband, of traditional SAs, such as semiconductor saturable absorber mirrors (SESAMs) and Fe^{2+}:ZnSe [8,9]. Therefore, the exploration of novel 2D materials for mid-infrared fiber laser pulse generation has been flourishing, and some encouraging results have been obtained [6,10–13].

Among various 2D materials, MXenes, a new series of 2D materials composed of transition metal carbides and/or carbonitrides with a generic chemical formula of $M_nX_{n+1}T_x$ ($n = 1$–3), has attracted rapid growing attention due to their distinctive and remarkable optical, electronic, and thermal properties. In the chemical formula, M represents an early transition metal [e.g., titanium (Ti), niobium (Nb), chromium (Cr), or molybdenum (Mo)], X denotes carbon and/or nitrogen, and T_x represents the surface functional group terminations (e.g., hydroxyl, oxygen, or fluorine) [14,15]. Being discovered lately, MXenes have already been intensively investigated both in theory and in experiments. In contrast to other (semiconducting or semimetal) 2D SAs reported, 2D MXenes (e.g., Ti_2C_3, Ti_3CN, Mo_2C) have been demonstrated to be metallic with high electron density near the Fermi level, which makes MXenes highly conductive [16]. Due to the metallic electronic band structure, their optical absorption can cover a broad wavelength region from near-infrared to mid-infrared, demonstrating the potential wideband SA applications [17–19]. Furthermore, MXenes are resilient with high damage thresholds and have very high melting points, excellent stability, as well as highly tunable and tailorable electronic/optical properties. In addition, the optoelectronic characteristics of MXenes

(e.g., $Ti_3C_2T_x$) have been proven to be sensitive not only to the type of surface termination but also to their orientation relative to MXene sheets [20]. All the above properties make MXenes highly suitable for effective nonlinear optical modulators for high power mid-infrared pulsed laser generation.

Recent studies with pulsed fiber lasers showed that MXenes (Ti_3CNT_x, Mo_2C, $Ti_3C_2T_x$, Ti_2CT_x) are excellent wideband SAs for laser pulse generations in the near-infrared spectral region with low linear losses and large modulation depths [18,20–23]. Jhon *et al.* presented a stable mode-locked fiber laser using Ti_3CN as an SA with an output power of 0.05 mW and a repetition rate of 15.4 MHz at 1557 nm [18]. Dong *et al.* experimentally characterized the nonlinear absorption of $Ti_3C_2T_x$ thin films at 1064 nm and showed a high modulation depth of up to ~50% and a high threshold of ~70 mJ · cm^{-2} for optical damage [24]. Very recently, Wang's group reported a 1.5 μm *Q*-switched Er^{3+}-doped fiber laser with an output power of 40 mW and pulse energy of 305 nJ based on $Ti_3C_2T_x$ [25]. Yi *et al.* reported a 2.8 μm stable *Q*-switched fiber laser with a maximum output power of 80 mW and pulse energy of 0.81 μJ using a Ti_2CT_x SA [23]. However, the saturable absorption properties around 3 μm, such as the modulation depth and saturable intensity, were not given. In addition, the average output power and pulse energy of the MXene SA reported in previous works are still below 100 mW and 1 μJ, respectively.

In this study, we demonstrated a watt-level high-efficiency passively *Q*-switched 2.8 μm mid-infrared fiber laser based on a MXene-$Ti_3C_2T_x$ SA. The 2786.2 nm passively *Q*-switched laser pulses with output power of 1.09 W and pulse energy of 13.93 μJ were realized. The multi-layered $Ti_3C_2T_x$ was prepared by selective etching of the aluminum layers in Ti_3AlC_2. The nonlinear absorption of the MXene-$Ti_3C_2T_x$ SA was characterized at 2866 nm using a homemade nonlinear absorption measurement system. The modulation depth, non-saturable loss, and saturable peak intensity were measured to be 33.2%, 25.0%, and 0.043 GW/cm^2, respectively. By employing the MXene-$Ti_3C_2T_x$ as the SA, we obtained 2786.2 nm passively *Q*-switched laser pulses with a pulse width of 1.04 μs at a repetition rate of 78.12 kHz. The slope efficiency was 28.23%. The maximum average power, pulse energy, and slope efficiency all represent the highest levels from a mid-infrared passively *Q*-switched fiber laser based on 2D materials.

2. PREPARATION AND CHARACTERIZATION OF MXENE-$Ti_3C_2T_x$

The multi-layered MXene-$Ti_3C_2T_x$ was prepared by etching the aluminum layers in Ti_3AlC_2 through a minimally intensive layer delamination (MILD) procedure. First, 2 g LiF was added into 40 mL of HCl (6 mol/L). After stirring at room temperature for ~5 min, 2 g of Ti_3AlC_2 was then added, and the mixture was continually stirred at 35°C for another 24 h. The flask covering was kept tight during the reaction to prevent the volatilization of HCl. After etching, the mixture was washed repeatedly by water (3 × 50 mL) until the pH value reached ~6. The mixture was then centrifuged at 3500 r/min for 1 h to obtain a multi-layered MXene-$Ti_3C_2T_x$ supernatant, which was further dip-coated onto the surface of a highly reflective gold mirror for further characterizations and applications.

After selective etching of the aluminum layers of Ti_3AlC_2, the prepared MXene-$Ti_3C_2T_x$ nanosheets showed a multi-layered structure with alternate Ti and carbon (C) layers in between and functional layers (i.e., O, F, and OH) on both sides (Fig. 1). The multi-layered $Ti_3C_2T_x$ nanosheets can be further delaminated to form few-layered or mono-layered MXene-$Ti_3C_2T_x$ (Fig. 1). The few-layered MXene-$Ti_3C_2T_x$ nanosheets were investigated by a transmission electron microscope (TEM) (Tecnai G2 F20) and an atomic force microscope (AFM) (BioScope Resolve). A thin wedge-shaped structure with ~200 nm length and ~80 nm width was observed in both TEM and AFM images [Figs. 2(a) and 2(b)]. The thickness of the nanosheets is well distributed between 5 and 6 nm, which are composed of only few layers [Fig. 2(b)]. The high-resolution TEM (HRTEM) (Tecnai G2 F20) image shows the inter-layer distance of the few-layered MXene-$Ti_3C_2T_x$ nanosheets of 9.87 Å, corresponding to (002) facets, which matches well with the previous theoretically calculated value (9.93 Å) [Fig. 2(c)] [26]. These indicated the successful fabrication of MXene-$Ti_3C_2T_x$ nanosheets.

Multi-layered MXene-$Ti_3C_2T_x$ nanosheets were used to prepare the MXene-$Ti_3C_2T_x$ on the surface. The morphologies and distributions were investigated by scanning electron microscopy (SEM) (JSM 7500F). The nanosheets were uniformly distributed on the substrate, indicating the MXene-$Ti_3C_2T_x$ shows homogeneous and stable absorbance on the surface [Fig. 2(d)]. An enlarged SEM image showed the accordion-like layered structure of the multi-layered $Ti_3C_2T_x$ nanosheets, which is in good accordance with the previous reports. The thickness of the multi-layered $Ti_3C_2T_x$ nanosheets was measured to be ~600 nm, which is ~100 times thicker than that of the few-layered $Ti_3C_2T_x$ nanosheets [Fig. 2(e)]. It is worthy to note that the $Ti_3C_2T_x$ with more layers has a stronger interaction with light than the few-layer or mono-layer structures [27,28]. The MXene-$Ti_3C_2T_x$ shows wide and flat absorption between 1500 nm and 3000 nm with an absorptivity absorbance of ~43% in the mid-infrared spectral region, indicating the potential to be an outstanding broadband optical modulator around 3 μm [Fig. 2(f)]. The small peak at ~2870 nm might result from the structure defection of the material.

The nonlinear absorption of $Ti_3C_2T_x$ was characterized by a typical power-dependent absorption measurement setup as shown in Fig. 3(a). The laser source was a homemade SESAM passively mode-locked Ho^{3+}/Pr^{3+} co-doped fluoride fiber

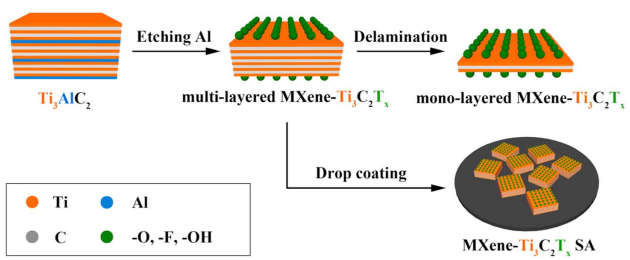

Fig. 1. Schematic illustration of fabricating multi-layered MXene-$Ti_3C_2T_x$, mono-layered MXene-$Ti_3C_2T_x$, and MXene-$Ti_3C_2T_x$ SA.

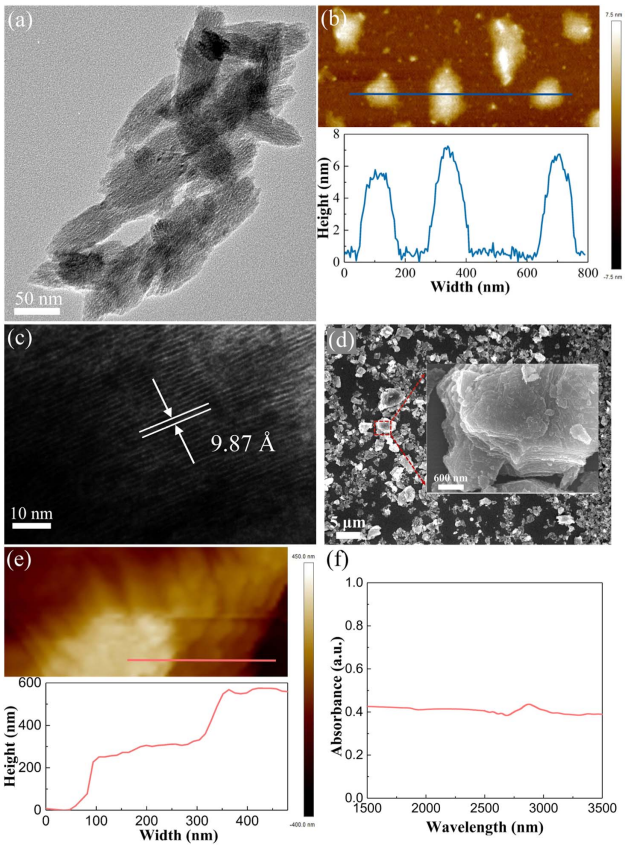

Fig. 2. (a) TEM image of the $Ti_3C_2T_x$ nanosheets on a scale of 50 nm. (b) AFM image of few-layered $Ti_3C_2T_x$ on a scale of 200 nm and the corresponding height profile. (c) HRTEM image of $Ti_3C_2T_x$ nanosheets on a scale of 10 nm. (d) SEM images of $Ti_3C_2T_x$ nanosheets on a scale of 5 μm and 600 nm (inset). (e) AFM image of multi-layered $Ti_3C_2T_x$ nanosheets on a scale of 200 nm and the corresponding height profile. (f) Linear absorption spectrum of $Ti_3C_2T_x$ powder.

laser with a center wavelength of 2866.0 nm, a pulse duration of ~20 ps, and a repetition rate of 17.86 MHz. A bandpass filter (FB2750-500, Thorlabs) was used to remove the residual 1150 nm pump laser. A gold (Au) mirror was utilized to steer the light. After that, a tunable diaphragm was used to continuously change the laser intensity radiated on the SA. A polarization beam splitter (PBS) with a 50:50 ratio was placed at an angle of 45° with respect to the light path to separate the laser source into two beams. The transmitted beam was focused on the $Ti_3C_2T_x$-coated Au mirror as the reflected power recorded by a power meter detector (Detector 1). The reflected beam was used as a reference power recorded by another power meter detector (Detector 2). By tuning the diaphragm, the reflectivity of the sample was calculated at various incident powers. Figure 3(b) shows the reflectivity as a function of pulse peak intensity. The experiment data was fitting with the formula:

$$R(I) = 1 - \Delta R \cdot \exp(-I/I_{sat}) - R_{ns}, \quad (1)$$

where $R(I)$ is the reflectivity, ΔR is the modulation depth, I is the incident peak intensity, I_{sat} is the saturable peak intensity, and R_{ns} is the non-saturable loss. The calculated modulation

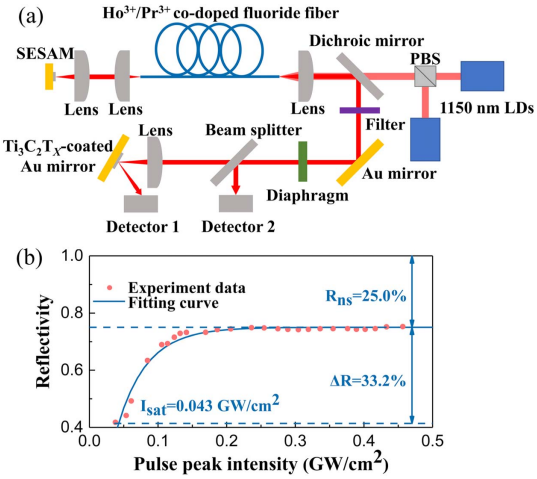

Fig. 3. (a) Experimental setup of nonlinear absorption measurement at 2866 nm. (b) Reflectivity of the $Ti_3C_2T_x$ sample as a function of pulse peak intensity.

depth, non-saturable loss, and saturable peak intensity are determined to be 33.2%, 25.0%, and 0.043 GW/cm^2, respectively.

3. EXPERIMENTAL SETUP

The schematic setup of the passively Q-switched Er^{3+}-doped ZBLAN fiber laser based on the MXene-$Ti_3C_2T_x$ SA is shown in Fig. 4. The pump light was provided by a 30 W fiber-coupled laser diode (LD) operated at 976 nm with a core diameter of 105 μm and a numerical aperture (NA) of 0.22. An aspheric condenser lens (L1) with a focal length of 16 mm was employed to collimate the pump light. For focusing the pump light into the first cladding of gain fiber, a CaF_2 plano-convex lens (L2) with a focal length of 20 mm was used. A 3.0 m double cladding Er^{3+}-doped ZBLAN fiber (Fiberlabs, Japan) with an erbium doping concentration of 60,000 ppm (parts per million) was used as the gain medium, which has a pump core with a diameter of 300 μm and an NA of 0.51 and a circular core with a diameter of 33 μm and an NA of 0.12. The fiber end facing the pump LD was perpendicularly cleaved to provide one cavity feedback with the help of 4% Fresnel reflection. The other end of the fiber was cleaved at an angle of 8° to avoid parasitic lasing. The laser beam from the angle-cleaved end was collimated by an AR-coated CaF_2 plano-convex lens (L3) with a focal length of 20 mm. A CaF_2 plano-convex lens (L4) with the same focal length was used to focus the laser onto the $Ti_3C_2T_x$-coated gold mirror (M2), which

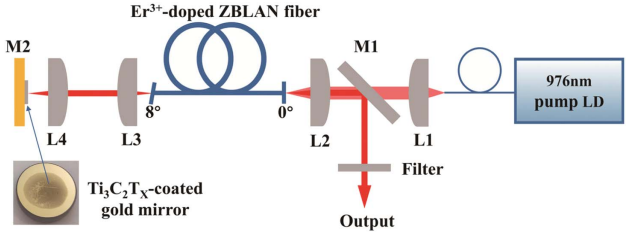

Fig. 4. Schematic setup of the passively Q-switched Er^{3+}-doped ZBLAN fiber laser based on the MXene-$Ti_3C_2T_x$ SA.

also provided the terminating cavity feedback. A dichroic mirror (M1) with 96% transmission at ~976 nm and 95% reflection at ~2.8 μm was placed between L1 and L2 at an angle of 45° with respect to the pump beam to steer the laser. The average power of the output laser beam was measured with a power meter (Laserpoint) along with a commercial 2.75 μm bandpass filter (FB2750-500, Thorlabs), which had a measured transmittance of ~84% at ~2.78 μm. The pulse train was captured by an indium arsenide (InAs) detector with a response time of 2 ns connected with a 500 MHz bandwidth digital oscilloscope. A monochromator with a scanning resolution of 0.1 nm (Princeton Instrument Acton SP2300) was utilized to measure the laser spectrum.

4. EXPERIMENTAL RESULTS AND DISCUSSION

The fiber laser started the *Q*-switching operation with a corresponding output power of 82.0 mW when the pump power was increased to 1.97 W. However, the pulse trains were unstable. It should be noted that the pump powers and the output powers mentioned here and below refer to the powers launched into the fiber and the average output powers, respectively. When the pump power increased to 2.72 W, a stable passively *Q*-switched pulse train was observed with a repetition rate of 32.47 kHz and a pulse width of 3.28 μs, as shown in Figs. 5(a) and 5(c). The *Q*-switched pulse train could maintain stability until the pump power reached 5.87 W. The corresponding repetition rate and pulse width were 78.12 kHz and 1.04 μs, respectively, as shown in Figs. 5(b) and 5(c). Once the pump power exceeded 5.87 W, the pulse train became unstable and then reverted to continuous-wave (CW) regime when the pump power grew to 6.03 W. This phenomenon was caused by the excessive heat accumulation of SA under strong signal laser [6,13,29]. At the pump power of 5.87 W, the optical and radio frequency (RF) spectra of the *Q*-switched pulses were measured as shown in Fig. 5(d) and the inset, respectively. The wavelength was centered at 2786.2 nm, and the full width at half maximum (FWHM) was about 2.3 nm. The signal-to-noise ratio (SNR) was 42.1 dB at the frequency of 78.12 kHz, which indicated a stable *Q*-switched operation.

Figure 6(a) depicts the average output power and pulse energy as functions of the pump power. The average output power increased almost linearly from 0.21 W to 1.09 W and the pulse energy raised from 6.52 μJ to 13.93 μJ when the pump power grew from 2.72 W to 5.87 W. Considering the

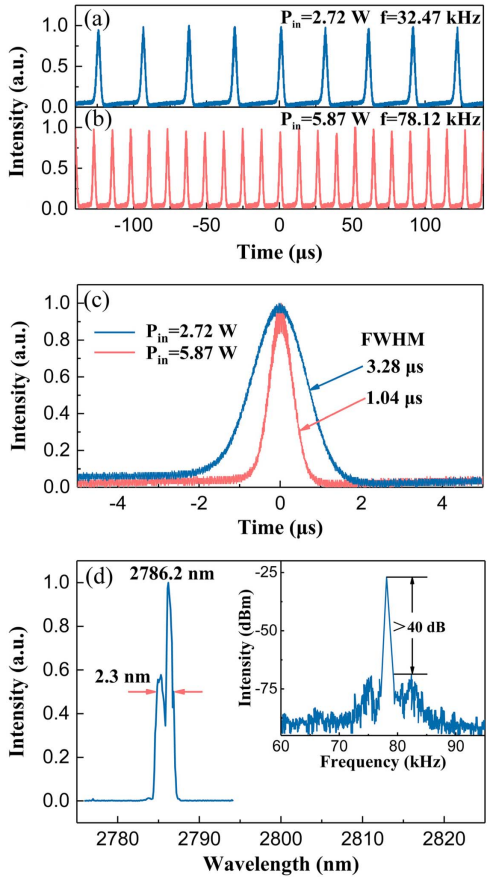

Fig. 5. *Q*-switched pulse trains at the pump power of (a) 2.72 W and (b) 5.87 W, (c) *Q*-switched single-pulse waveforms at the pump power of 2.72 W and 5.87 W, and (d) optical and RF (inset) spectra of the *Q*-switched pulses at the pump power of 5.87 W.

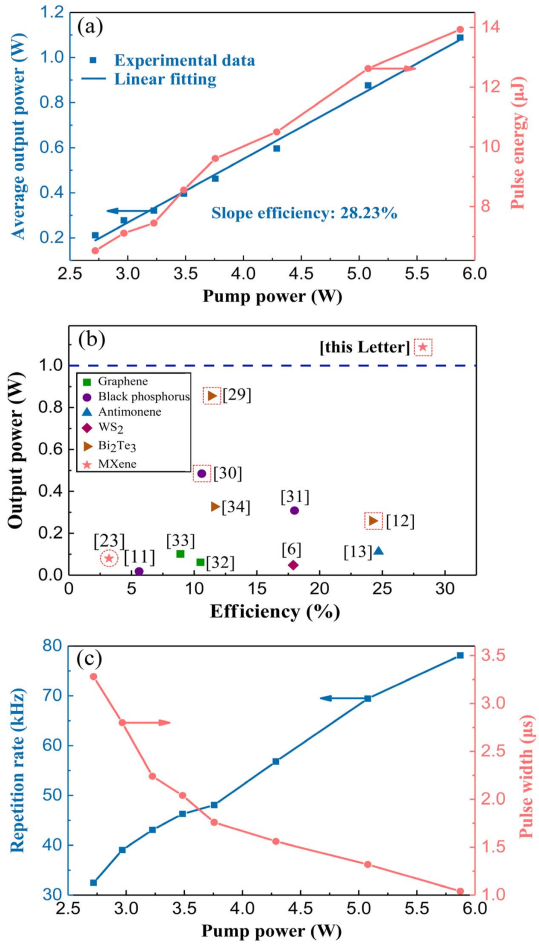

Fig. 6. (a) Output power and single-pulse energy as functions of the pump power, (b) output powers and slope efficiencies of mid-infrared passively *Q*-switched fiber lasers with different 2D materials SAs (icons with squares: multi-mode; icons with circles: mode unknown; icons without framing: single mode), and (c) repetition rate and pulse width as functions of the pump power.

33 μm core diameter of the gain fiber (cutoff wavelength 5.2 μm), the pulsed laser was operating in multi-mode. The stable *Q*-switched operation with average output power as high as 1.09 W indicates the high damage threshold of the SA. The slope efficiency of this laser system was measured to be 28.23%. Such high slope efficiency could be mainly attributed to the low insertion loss of the SA and the compact cavity design. Figure 6(b) gives a summary of the output powers and slope efficiencies from the previously demonstrated 2D materials-enabled mid-infrared passively *Q*-switched fiber lasers [6,11–13,23,29–34]. We can see from Fig. 6(b) that both the output power and slope efficiency achieved from this work are the highest. Figure 6(c) shows the measured repetition rate and pulse width as functions of the pump power. The repetition rate increased from 32.47 kHz to 78.12 kHz, while the pulse width decreased from 3.28 μs to 1.04 μs. Accordingly, the highest peak intensity was calculated to be 19.13 kW/cm^2.

In our experiment, when the pump power reached 7.98 W, which is the highest pump power we used to prevent the end facet degradation in the optical fiber due to heat accumulation, the laser was still operating in the CW regime. We then decreased the pump power back to around 5.87 W, and stable *Q*-switched pulses with the same average power, repetition rate, and pulse duration as before were observed again, indicating that the MXene-$Ti_3C_2T_x$ SA was not damaged, which also verified the high optical damage threshold of MXene-$Ti_3C_2T_x$. However, we have not observed mode-locked operation of this fiber laser in our experiment. This may result from the un-optimized parameter range of the MXene-$Ti_3C_2T_x$ SA and/or the current laser resonator design. Further investigation into the mode-locked operation of mid-infrared fiber lasers by optimizing the linear and nonlinear absorption of the MXene-$Ti_3C_2T_x$ and increasing the *Q* factor of the optical laser resonator is currently underway.

5. CONCLUSION

In conclusion, we experimentally investigated the saturable absorption property of $Ti_3C_2T_x$ at 2866 nm and revealed its potential as a superior SA in the 3 μm mid-infrared region. We present the first, to the best of our knowledge, watt-level passively *Q*-switched 2.8 μm mid-infrared fiber laser based on 2D materials. The calculated modulation depth, non-saturable loss, and saturable peak intensity of the as-prepared $Ti_3C_2T_x$ are 33.2%, 25.0%, and 0.043 GW/cm^2, respectively. The maximum pulse energy of 13.93 μJ at a repetition rate of 78.12 kHz and a high slope efficiency of 28.23% were obtained. This work indicates that MXene-$Ti_3C_2T_x$ is a reliable and superior broadband SA for high power mid-infrared pulsed laser generation.

Funding. National Natural Science Foundation of China (61875033, 61705147, 61775031, 61421002); Chengdu Science and Technology Huimin Project (2016-HM01-00269-SF, 2016-HM01-00265-SF); Fundamental Research Funds for the Central Universities (YJ201654).

Disclosures. The authors declare that there are no conflicts of interest related to this paper.

REFERENCES

1. F. K. Tittel, D. Richter, and A. Fried, "Mid-infrared laser applications in spectroscopy," in *Solid-State Mid-Infrared Laser Sources*, I. Sorokina and K. Vodopyanov, eds. (Springer, 2003).
2. H. H. P. Th. Bekman, J. C. van den Heuvel, F. J. M. van Putten, and R. Schleijpen, "Development of a mid-infrared laser for study of infrared countermeasures techniques," Proc. SPIE **5615**, 27–38 (2004).
3. M. C. Pierce, S. D. Jackson, M. R. Dickinson, T. A. King, and P. Sloan, "Laser-tissue interaction with a continuous wave 3-μm fibre laser: preliminary studies with soft tissue," Lasers Surg. Med. **26**, 491–495 (2000).
4. D. J. Richardson, J. Nilsson, and W. A. Clarkson, "High power fiber lasers: current status and future perspectives [Invited]," J. Opt. Soc. Am. B **27**, B63–B92 (2010).
5. R. I. Woodward, M. R. Majewski, and S. D. Jackson, "Mode-locked dysprosium fiber laser: picosecond pulse generation from 2.97 to 3.30 μm," APL Photon. **3**, 116106 (2018).
6. C. Wei, H. Luo, H. Zhang, C. Li, J. Xie, J. Li, and Y. Liu, "Passively *Q*-switched mid-infrared fluoride fiber laser around 3 μm using a tungsten disulfide (WS_2) saturable absorber," Laser Phys. Lett. **13**, 105108 (2016).
7. C. Frerichs and U. B. Unrau, "Passive *Q*-switching and mode-locking of erbium-doped fluoride fiber lasers at 2.7 μm," Opt. Fiber Technol. **2**, 358–366 (1996).
8. J. F. Li, H. Y. Luo, Y. L. He, Y. Liu, L. Zhang, K. M. Zhou, A. G. Rozhin, and S. K. Turistyn, "Semiconductor saturable absorber mirror passively *Q*-switched 2.97 μm fluoride fiber laser," Laser Phys. Lett. **11**, 065102 (2014).
9. C. Wei, X. Zhu, R. A. Norwood, and N. Peyghambarian, "Passively *Q*-switched 2.8 μm nanosecond fiber laser," IEEE Photon. Technol. Lett. **24**, 1741–1744 (2012).
10. G. Zhu, X. Zhu, F. Wang, S. Xu, Y. Li, X. Guo, K. Balakrishnan, R. A. Norwood, and N. Peyghambarian, "Graphene mode-locked fiber laser at 2.8 μm," IEEE Photon. Technol. Lett. **28**, 7–10 (2016).
11. Z. Qin, G. Xie, J. Ma, P. Yuan, and L. Qian, "2.8 μm all-fiber *Q*-switched and mode-locked lasers with black phosphorus," Photon. Res. **6**, 1074–1078 (2018).
12. J. Liu, M. Wu, B. Huang, P. Tang, C. Zhao, D. Shen, D. Fan, and S. K. Turitsyn, "Widely wavelength-tunable mid-infrared fluoride fiber lasers," IEEE J. Sel. Top. Quantum Electron. **24**, 0900507 (2018).
13. H. Luo, X. Tian, Y. Gao, R. Wei, J. Li, J. Qiu, and Y. Liu, "Antimonene: a long-term stable two-dimensional saturable absorption material under ambient conditions for the mid-infrared spectral region," Photon. Res. **6**, 900–907 (2018).
14. M. Naguib, M. Kurtoglu, V. Presser, J. Lu, J. Niu, M. Heon, L. Hultman, Y. Gogotsi, and M. W. Barsoum, "Two dimensional nanocrystals produced by exfoliation of Ti_3AlC_2," Adv. Mater. **23**, 4248–4253 (2011).
15. M. Naguib, O. Mashtalir, J. Carle, V. Presser, J. Lu, L. Hultman, Y. Gogotsi, and M. W. Barsoum, "Two-dimensiona transition metal carbides," ACS Nano **6**, 1322–1331 (2012).
16. I. R. Shein and A. L. Ivanovskii, "Graphene-like titanium carbides and nitrides $Ti_{n+1}C_n$, $Ti_{n+1}N_n$ (n=1, 2, and 3) from de-intercalated MAX phases: first-principles probing of their structural, electronic properties and relative stability," Comput. Mater. Sci. **65**, 104–114 (2012).
17. Y. Xie and P. R. C. Kent, "Hybrid density functional study of structural and electronic properties of functionalized $Ti_{n+1}X_n$ (X=C, N) monolayers," Phys. Rev. B **87**, 235441 (2013).
18. Y. Jhon, J. Koo, B. Anasori, M. Seo, J. H. Lee, Y. Gogotsi, and Y. M. Jhon, "Metallic MXene saturable absorber for femtosecond mode-locked lasers," Adv. Mater. **29**, 1702496 (2017).
19. Y. C. Dong, S. Chertopalov, K. Maleski, B. Anasori, L. Hu, S. Bhattacharya, A. M. Rao, Y. Gogotsi, V. N. Mochalin, and R. Podila, "Saturable absorption in 2D Ti_3C_2 MXene thin films for passive photonic diodes," Adv. Mater. **30**, 1705714 (2018).
20. M. Hu, T. Hu, Z. Li, Y. Yang, R. Cheng, J. Yang, C. Cui, and X. Wang, "Surface functional groups and interlayer water determine the electrochemical capacitance of $Ti_3C_2T_x$ MXene," ACS Nano **12**, 3578–3586 (2018).
21. M. Tuo, C. Xu, H. Mu, X. Bao, Y. Wang, S. Xiao, W. Ma, L. Li, D. Tang, H. Zhang, M. Premaratne, B. Sun, H. Cheng, S. Li, W. Ren, and

Q. Bao, "Ultrathin 2D transition metal carbides for ultrafast pulsed fiber lasers," ACS Photon. **5**, 1808–1816 (2018).
22. X. Jiang, S. Liu, W. Liang, S. Luo, Z. He, Y. Ge, H. Wang, R. Cao, F. Zhang, Q. Wen, J. Li, Q. Bao, D. Fan, and H. Zhang, "Broadband nonlinear photonics in few-layer MXene $Ti_3C_2T_x$ (T=F, O, or OH)," Laser Photon. Rev. **12**, 1700229 (2018).
23. J. Yi, L. Du, J. Li, L. Yang, L. Hu, S. Huang, Y. Dong, L. Miao, S. Wen, V. N. Mochalin, C. Zhao, and A. M. Rao, "Unleashing the potential of Ti_2CT_x MXene as a pulse modulator for mid-infrared fiber lasers," 2D Mater. **4**, 045038 (2019).
24. Y. Dong, S. Chertopalov, K. Maleski, B. Anasori, L. Hu, S. Bhattacharya, A. M. Rao, Y. Gogotsi, V. N. Mochalin, and R. Podila, "Saturable absorption in 2D Ti_3C_2 MXene thin films for passive photonic diodes," Adv. Mater. **30**, 1705714 (2018).
25. L. Wang, X. Li, C. Wang, W. Luo, T. Feng, Y. Zhang, and H. Zhang, "Few-layer Mxene $Ti_3C_2T_x$ (T=F, O, or OH) for robust pulse generation in a compact Er-doped fiber laser," ChemNanoMat **5**, 1233–1238 (2019).
26. C. Shi, M. Beidaghi, M. Naguib, O. Mashtalir, Y. Gogotsi, and S. J. Billinge, "Structure of nanocrystalline Ti_3C_2 MXene using atomic pair distribution function," Phys. Rev. Lett. **112**, 125501 (2014).
27. J. Zhang, D. H. Li, R. J. Chen, and Q. H. Xiong, "Laser cooling of a semiconductor by 40 kelvin," Nature **493**, 504–508 (2013).
28. D. H. Li, J. Zhang, and Q. H. Xiong, "Laser cooling of CdS nanobelts: thickness matters," Opt. Express **21**, 19302–19310 (2013).
29. P. Tang, M. Wu, Q. Wang, L. Miao, B. Huang, J. Liu, C. Zhao, and S. Wen, "2.8 μm pulsed Er^{3+}:ZBLAN fiber laser modulated by topological insulator," IEEE Photon. Technol. Lett. **28**, 1573–1576 (2016).
30. Z. Qin, G. Xie, H. Zhang, C. Zhao, P. Yuan, S. Wen, and L. Qian, "Black phosphorus as saturable absorber for the *Q*-switched Er:ZBLAN fiber laser at 2.8 μm," Opt. Express **23**, 24713–24718 (2015).
31. J. Li, H. Luo, B. Zhai, R. Lu, Z. Guo, H. Zhang, and Y. Liu, "Black phosphorus: a two-dimension saturable absorption material for mid-infrared *Q*-switched and mode-locked fiber lasers," Sci. Rep. **6**, 30361 (2016).
32. C. Wei, X. Zhu, F. Wang, Y. Xu, K. Balakrishnan, F. Song, R. A. Norwood, and N. Peyghambarian, "Graphene *Q*-switched 2.78 μm Er^{3+}-doped fluoride fiber laser," Opt. Lett. **38**, 3233–3236 (2013).
33. G. Zhu, X. Zhu, K. Balakrishnan, R. A. Norwood, and N. Peyghambarian, "Fe^{2+}:ZnSe and graphene *Q*-switched singly Ho^{3+}-doped ZBLAN fiber lasers at 3 μm," Opt. Mater. Express **3**, 1365–1377 (2013).
34. J. Li, H. Luo, L. Wang, C. Zhao, H. Zhang, H. Li, and Y. Liu, "3-μm mid-infrared pulse generation using topological insulator as the saturable absorber," Opt. Lett. **40**, 3659–3662 (2015).